University Jaume I
Department of Inorganic and Organic Chemistry
Solid State Chemistry Group

Bachelor Thesis

Synthesis of $CuIn_xGa_{(1-x)}Se_2$ semiconductor as a absorber for thin film solar cells

by

Jose Pedro Sales

Supervisor: Dra. Teodora Stoyanova Lyubenova

Mentor: Rafael Martí Valls

September 2015
Castellón

INDEX

Chapter-1

Chapter-2

Chapter-1

I. Introduction

I.1 Fuels vs. renewable energies

In our global society, it simply means energy that is produced from sources other than our primary energy supply: fossil fuels. Coal, oil and natural gas are the three kinds of fossil fuels that we have mostly depended on for our energy needs, from home heating and electricity to fuel for our automobiles and mass transportation. They also induce a negative environmental impact by generating lots of polluting by-products. Burning fossil fuels creates carbon dioxide that contributes to a global warming. Combustion of these fossil fuels is considered to be the largest contributing factor to the release of greenhouse gases into the atmosphere. In the 20th century, the average temperature of Earth rose 1 degree Fahrenheit (1°F). This period saw the most prolific population growth and industrial development (which was and remains totally dependent on the use of energy) in Earth's history. The impact of global warming on the environment is extensive and affects many areas. In the Arctic and Antarctica, warmer temperatures are causing the ice to melt which will increase sea level and change the composition of the surrounding sea water. Rising sea levels alone can impede processes ranging from settlement, agriculture and fishing both commercially and recreationally. Air pollution is also a direct result of the use of fossil fuels, resulting in smog and the degradation of human health and plant growth.

The problem is that the fossil fuels are non-renewable. They are also limited in supply and one day will be depleted. Nowadays, there no guarantee that this fuels will be enough to satisfy the long term increasing energy demand generated by the growth of population and industry. This situation has generated a worldwide interest in finding alternative energy sources, preferably renewable.

Sun, wind and water are perfect energy sources (depending on where you are). They are non-polluting, renewable and efficient. All you need is sunlight, running water and/or wind to create electricity. The use of renewable energy sources helps to reduce the global carbon dioxide emissions. They also add some much-needed flexibility to the energy resource by decreasing our dependence on limited reserves of fossil fuels.

Essentially, these renewable energy sources create their own energy. The object is to capture and harness their mechanical power and convert it to electricity in the most effective and productive manner possible. There's more than enough renewable energy sources to supply all of the world's energy needs forever; however, the challenge is to develop the capability to effectively and economically capture, store and use the energy when needed.

The main aim of this project is to create suitable photo-absorber semiconducting material for photovoltaic applications. The definite objectives are discussed in Chapter 2.

I.2 Solar cells technology

Currently, the global photovoltaic (PV) technology is increasing dramatically. Over the past 20 years, manufacturing output has grown by a factor of 200, reaching 5 gigawatts (GW) in 2008. The total accumulated installed capacity is now around 15 GW. This is quite small relative to the world's 4000 GW of installed electric generation capacity just 0.375% to be precise. However, industry leaders expect similar rapid growth over the coming years, with PV generation a major contributor to power generation 20 years hence [1].

The understanding of photo-processes involving semiconductors require, in turn, an understanding of the primary mechanisms of charge-carrier generation and mobility in these materials. In a bulk crystalline semiconductor, the highest occupied and lowest unoccupied molecular orbitals (HUMO and LUMO) of constituent atoms or molecules converge into valance and conduction bands. In the absence of dopants, the energy level (Fermi level) of the semiconductor lies half-way between the separation gap of the valence and conduction bands. Doping with electron-donors (n-doping) makes the material electron-rich, and the Fermi level moves closer to the valance band. Similarity, doping with electron-acceptors (p-doping) depletes the number of electrons available and the Fermi level moves closer to the valance band. Optical excitation of the semiconductor with light of energy higher than the bandgap separation of the semiconductor leads to generation of free charge carriers, electrons (e^-) and holes (h^+). In a sandwich structure composed of an n-doped and p-doped semiconductor, charge separation occurs due to bending of the bands in the vicinity of the interface (see Fig.1)

With light additional carriers are created, and the single Fermi level splits into two quasi-Fermi levels in the n-type or p-type region respectively. These quasi-Fermi levels are now split; the higher the light intensity the more they split. Close to the electrode both quasi-Fermi levels collapse toward the majority quasi-Fermi level, where they are connected [2].

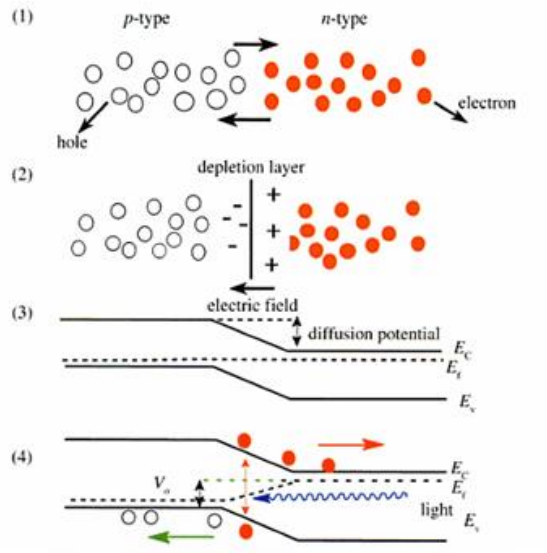

Figure 1. Band picture of n- and p-type semiconductors with indication of the Fermi level (E_1) before (scheme 1) and after joining (scheme 2) resulting in a p-n junction

This shift of the Fermi levels in the electrodes represents the open circuit voltage, which can be approximated by the shift of the minority quasi-Fermi levels. Such separation of the charge carriers permits selective collection at the collector electrodes and a net conversion of sunlight to electric power.

Based on the nature of the material, maximum conversion efficiency obtainable, and the associated cost of photovoltaic power, Martin Green has grouped various photovoltaic solar cells in three major categories (see Fig.2).

- ***First generation Photovoltaic*** uses the highest purity materials with least structural defects (such as single crystals). The highest power-conversion efficiencies obtained to date are in first generation PVs. Due to high labor costs for the material processing and the significant energy input required, cost per watt is also the highest. It is very unlikely that these systems will allow photoelectric power conversion for less than 1 US$/watt. In addition to single component Si and layered semiconductors, binary semiconductors of II-IV and III-V have been examined.

- ***Second generation devices*** are based on low-energy, intensive preparation techniques such as vapor deposition and electroplating. Since it is difficult to prepare systems without defects, maximum power conversion is lower. Nearly all thin film photovoltaic fall in this category, and the power cost can be less than 1 US$/watt. Most efficient examples are solar cells made up of multi-crystalline or amorphous Si, CdTe and Cd-In-Ga-Se (CIGS). Table 1 provides a summary of the state of the art conversion efficiency reported for various semiconductor-based solar cells of the first and second generations. These materials are applied as a thin film to a supporting substrate such as glass or ceramics, reducing material mass and therefore costs.

Table 1. Summary of the conversion efficiency reported for various semiconductor-based solar cells of the first and second generations

PV material	Efficiency (%)	Area (cm^2)	V_{OC} (V)	I_{SC} (ma/cm^2)	*FF* (%)	Lab, year
Si (crystalline)	25.0 ± 0.5	4.00	0.705	42.7	82.8	Sandia 1999
Si (multicryst.)	20.4 ± 0.4	1.002	0.664	38.0	80.9	NREL 2004
Si (thin film)	16.7 ± 0.4	4.017	0.645	33.0	78.2	FhG-ISE 2001
Si (thin film)	10.5 ± 0.3	94.0	0.492	29.7	72.1	FhG-ISE 2007
GaAs (cryst.)	26.1 ± 0.8	0.998	1.038	29.7	84.7	FhG-ISE 2007
GaAs (thin film)	26.1 ± 0.8	1.001	1.045	29.5	84.6	FhG-ISE 2008
GaAs (multicryst.)	18.4 ± 0.5	4.011	0.994	23.2	79.7	NREL 1995
InP (cryst.)	22.1 ± 0.7	4.02	0.878	29.5	85.4	NREL 1990
CIGS (cell)	19.4 ± 0.6	0.994	0.716	33.7	80.3	NREL 2008
CIGS (sub-module)	16.7 ± 0.4	16.0	0.661	33.6	75.1	FhG-ISE 2000
CdTe (cell)	16.7 ± 0.5	1.032	0.845	26.1	75.5	NREL 2001
Si (amorph.)	9.5 ± 0.3	1.070	0.859	17.5	63.0	NREL 2003
Si (nanocryst.)	10.1 ± 0.2	1.199	0.539	24.4	76.6	JQA 1997
Dye-sensitized (sub-module)	10.4 ± 0.3	1.004	0.729	22.0	65.2	AIST-Sharp 2005
Dye-sensitized (sub-module)	8.2 ± 0.3	25.45	0.705	19.1	61.1	AIST–Sharp 2007
Dye-sensitized (sub-module)	8.2	18.50	0.659	19.9	62.9	AIST-Sony 2008
Org. polymer	5.15	1.021	0.876	9.39	62.5	NREL 2006
Organic (sub-module)	1.1	232.8	29.3	0.072	51.2	NREL 2008

There have been several theoretical calculations on maximum power conversion obtainable using solar radiation. The most popular calculation is that of Shockley and Queisser. Considering photovoltaic solar cells as a one-photon giving one-electron threshold device, these authors estimate 31% as maximum under 1 sun illumination and 40,8% under maximal concentrated solar light (46.200 suns). During the past decade several approaches have been suggested to cut down the energy losses and increase the overall conversion.

In one classification, all photovoltaic systems that can potentially give power conversion efficiency over and above the Shockley and Queisser limit are labeled as ***third generation photovoltaic***. Advances in our understanding of solid-solid and solid-liquid interfaces of various kinds permit noe usage of wide variety of quasi-crystalline and even amorphous materials made out of monodispersed colloids, polymers, gels and electrolytes. Since there is excellent potential for these photovoltaic systems, based on novel materials and nanotechnology, to deliver solar electric power at very low costs (0,1-0,5 $US/watt), solar cells based on dye-sensitization, polymer organic-bulk hetero-junctions, and quantum dots are also referred to as third-generation PV systems [2].

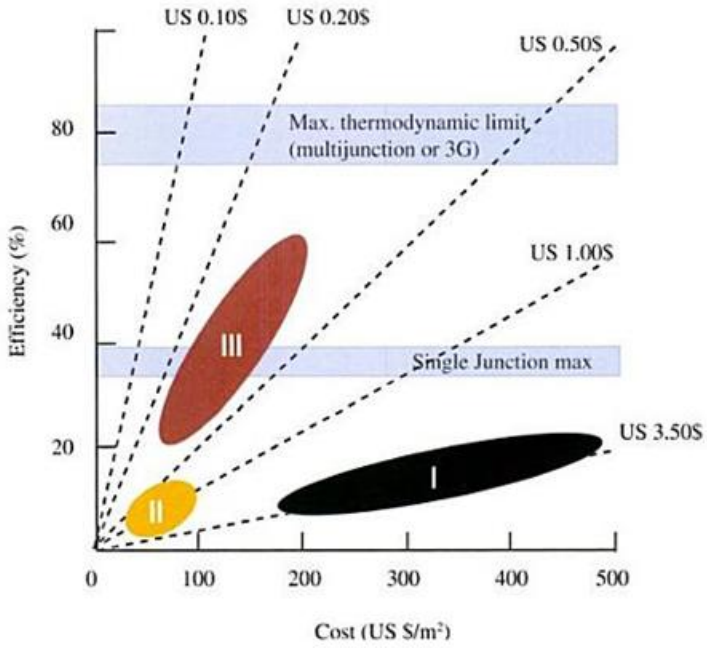

Figure 2. Classification of photovoltaic solar cells into three categories, based on the nature of the materials used and associated cost of electric power generation [2].

I.3 $CuIn_xGa_{(1-x)}Se_2$ (CIGS)

This photovoltaic system has been considered one of the most promising solar cell technologies for cost-effective power generation [3]. There are many reasons for this. On one hand this technology has demonstrated high and stable efficiency- about 20% [4], close to that of crystalline silicone. On the other, the inherent advantages of thin-film processing, in contrast to bulk crystalline materials, permits quick upscale of the deposition process to high-throughput, large area deposition. Another big advantage of thin-film technologies is the possibility to replace the individual cell processing and soldering procedure of silicon wafers with simple scribing. This can provide straightforward monolithic interconnection of individual cells and results in high module output voltage and reduced series resistance losses. Several companies have already

started pilot production of large-area modules, yielding efficiency above 12%. The record of 13.4% full-scale module belongs to Showa Shell [5].

The history of this technology starts with the synthesis of $CuInSe_2$ by Hahn in 1953 [6]. The first photovoltaic device was fabricated from a single crystal with 12% efficiency in 1974 [7]. Boeing Corporation developed the first efficient (10%) thin-film devices in the early 80-s by use of a process based on three-source co-evaporation [8]. With some modifications (multistage instead of two-stage regime) it is still the record-performance process used today both for cells and modules. In 1987 Arco Solar increased this efficiency to 14% [9].The same company under the name Siemens Solar (later Shell Solar) produced the first commercial chalcopyrite photovoltaic module in1998 [10]. Today numerous companies, employing various processes, materials and substrates are involved in intense development work to scale up their pilot facilities to large-scale production. Some of them use vacuum-based techniques such as sputtering or co-evaporation: Wurth Solar, Avancis, Showa Shell, Miosole, HelioVolt, Global Solar, Sulfurcell, etc. At the same time there are already companies which introduce at the industrial level novel low-cost vacuum-free approaches. Institut de Recherche et Développement sur l'Énergie Photovoltaïque (IRDEP) and Solopower use electro-deposition. International Solar Electric Technology (ISET) and Nanosolar employ nanoparticle suspension printing.

Quick growth of production volumes is envisioned in the near future as many of the processes have reached maturity and large production facilities are under construction. Three main issues still have to be addressed by researchers:

- Lower processing costs and higher efficiency by vacuum-free deposition routes.
- Replacement of toxic elements such as selenium and cadmium employed by current technology.
- Replacement of rare elements such as indium and gallium with more abundant alternatives.

If these issues are properly addressed, the chalcopyrite photovoltaic technology has unlimited potential to supply our civilization with cheap and abundant renewable energy.

I.3.1 Device structure and operation

While there is a large variety of processes and materials used for the fabrication of chalcopyrite devices. . The main components of these types of solar cells are shown in Figure 3.
This structure includes 5 principal elements which are:

- **Substrate** – usually soda lime glass, providing adequate surface for the deposition of the active layers. Other materials as metal and plastic are also used. CIGS efficiencies related with the substrate used are listed in the Table 2.
- **Back contact** - sputtered molybdenum is the most frequency used metallic contact.
- **Absorber** – p-type chalcopyrite $Cu(In,Ga)Se_2$or $Cu(In,Ga)(Se, S)_2$
- **Buffer** – n-type CdS
- **Transparent conductive oxide** – Al-doped ZnO (often preceded by a thinner isolating ZnO)

Table 2. Lab record CIGS efficiencies by substrate

Substrate	Glass	Steel	Aluminum	Polymer
Efficiency	20.8%	17.7%	16.2%	20.4%
Institute	ZSW [b]	Empa	Empa	Empa

Source: Swissolar, Flisom – presentation November 2014[22]

Note: [a] lab cell with ~0.5 cm^2, [b] ZSW: Zentrum für Sonnenenergie- und Wasserstoff-Forschung

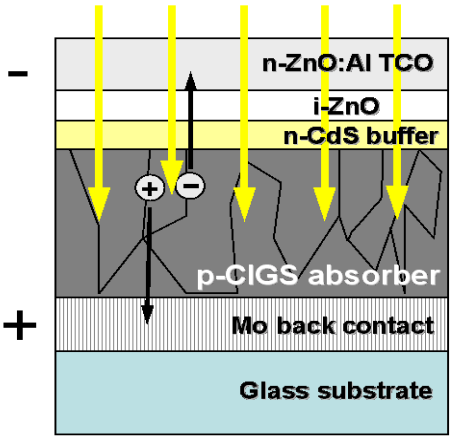

Figure 3 Structure of a record-performance chalcopyrite device.

In contrast to the CdTe solar cells, which are built in superstrate configuration (i.e. by depositing all layers on transparent material that is intended to face the illuminated side), the general process for chalcopyrite devices employs the substrate version. Several research efforts have demonstrated the feasibility of superstrate version of $Cu(In,Ga)Se_2$ cells but the efficiency was substantially lower than substrate devices [11]. Although superstrate-type solar cells can potentially be used asthe top cell of tandem (multi-junction) devices and there are made by lowering manufacturing costs, the efficiencies of these cells still remain in the 10–12% range [12].

The main advantage of the substrate junction is the possibility to grow the absorber at higher temperature without damaging the p-n junction. Its subsequent formation is easily achieved by a variety of routes at low temperature. Subjecting the junction to temperatures above 200ºC can have negative impact on performance.

A brief review of the principal cell elements is given below.

A) Substrate

The best-studied substrate is soda lime glass. It was originally used because of its low cost, chemical inertness and thermal stability. Soon it was found out that very small amounts of sodium diffusing from the glass into the absorber have beneficial effect on its electronic properties. Advanced processes use sodium diffusion barrier and later deposit controlled amount of sodium compound in order to achieve better control on Na-incorporation [13].

Flexible substrates are of particular interest from industrial point of view because of the possibility of using roll-to-roll processing. Different materials such as metal and

polymeric foils have been used. There are several requirements to the substrate which make it difficult to find an optimal flexible substrate [14]:

• Vacuum compatibility. The substrate should not degas during the various vacuum deposition steps, especially during CIGS deposition, when the substrate must be heated. This requirement is not valid for low-cost, vacuum-free deposition methods.

• Thermal stability. Generally, efficient devices are grown at temperatures exceeding 400ºC, while record performance CIGS is deposited at temperatures about 550ºC. Polymeric foils are not suitable for temperatures above 450ºC.

• Suitable coefficient of thermal expansion (CTE). It should match the one of the absorber (7-11 ppm/K) as closely as possible, otherwise poor adhesion or molybdenum cracking may be observed. While titanium and steel foils have similar CTE (8.6 and 11ppm/K respectively), the values for aluminum (23ppm/K) and many polymers are very high and result in absorber delamination.

• Chemical inertness. The substrate should not be damaged while exposed to the different aggressive processing environments, in particular to Se environment at high temperature during the absorber formation and in the chemical bath used for buffer deposition. In addition, it should not release impurities that may deteriorate the electronic properties of the cell, except when this is explicitly desired (such as in the case of Na diffusing from the soda lime glass). In some cases a diffusion barrier can be deposited in order to meet this requirement.

• Sufficient humidity barrier. Because long-term atmospheric exposure (especially at high temperature and humidity) may damage the modules, the substrate must provide reliable atmospheric protection.

• Surface smoothness. Substrate roughness, especially at micrometric scale may result in shunting the front and back contact. At the same time, isolation scribing required for module interconnection cannot be performed successfully on rough substrates.

• Cost, energy consumption, availability, weight. These general requirements apply to all module elements, especially if large-scale deployment is envisioned.

B) Back contact

The most widely used back contact for chalcopyrite devices is sputtered molybdenum layer. It has several advantages such as:

- Low reactivity with chalcogens during absorber deposition
- Coefficient of thermal expansion close to the absorber
- High hardness, permitting mechanical scribing of the subsequent layers for module interconnection without damaging the contact.

Often a thin layer of $MoSe_2$ forms during the high temperature treatments of the buffer. This phenomenon is normally not detrimental for cell performance.

In some cases, when a metallic foil is used, it is possible to omit the back contact deposition and cut single cells which are then interconnected in series similarly to silicon solar cells. Nevertheless, impurities that could diffuse from the foil may require a deposition of an additional diffusion barrier. Such interconnections are used by some companies employing low-cost processing such as ISET and Nanosolar. However, one of the biggest advantages of thin-film modules is the easy monolithic series interconnection on a single large substrate. This is why ongoing research efforts on

flexible substrates are focused on non-conductive (polymeric and inorganic) materials or reliable isolation of metallic foils. Subsequent deposition of molybdenum film provides the classical configuration back contact.

Another type of back contact, especially interesting for the fabrication of semi-transparent or stacked junction devices is the transparent back contact. Employing transparent conductive oxides, SnO:F and ITO (indium-tin oxide), device efficiencies of 13.7 and 15.2% were reached [15].

C) Absorber layer

This is the most important layer of the chalcopyrite device and has been a subject to a vast array of research activities, resulting in numerous modifications and improvements. As already mentioned, record performance has been achieved with $Cu(In,Ga)Se_2$, although many other materials are being investigated.

In all cases the absorber formation is based on delivery of the constituting elements by a vacuum or atmospheric pressure technique, accompanied or followed by high-temperature treatment resulting in crystalline material.

Low-cost atmospheric pressure approaches for absorber formation are one of the major objectives of this thesis.

Another challenge for CIGS technology related to large-scale production is the substitution of the scarce and toxic elements such as In, Ga and Se with environmentally friendly and abundant alternatives. An example of a promising material is Cu_2ZnSnS_4 which was successfully deposited by a low-cost method in this work.

The project consists in the development of absorber layers using low-cost methods (without vacuum).

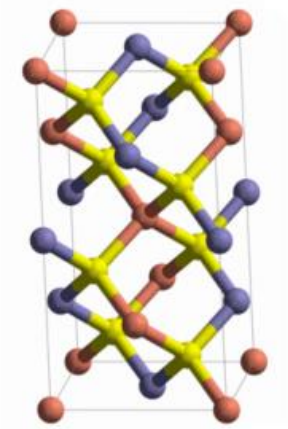

Figure 4. Chalcopyrite structure CIGS (red= Cu, yellow= Se, blue= In/Ga)

D) Buffer layer

Serving also as the n-partner in the p-n hetero junction, this layer is crucial for cell performance. It is very thin (10-60nm) and has to provide complete coverage of the absorber.

While there are numerous and sometimes controversial reports on how the buffer contributes to device efficiency enhancement [16, 17], there is a general agreement that it chemically modifies the absorber surface and, in addition, provides protection of the absorber surface during ZnO sputtering.

Record performing devices employ CdS buffer layers deposited by chemical bath deposition. Both the material itself and its formation route are undesirable for industrial production. Apart from being a relatively slow, precisely controlled batch process, CBD has the following inherent disadvantages: a need for fresh solution for each cycle, poor material utilization and necessity to manage large amounts of residual liquids.

Intense research efforts by many teams have yielded fundamental understanding and successful alternatives of CdS, in most cases by use of zinc or indium sulfide based materials. Good results in large-scale experiments have been achieved with methods alternative to CBD, such as atomic layer deposition (ALD), metal organic chemical vapor deposition (MOCVD), ion layer gas reaction (ILGAR), sputtering and thermal evaporation [18]. However, most of these methods still need to be approved in industry.

E) Transparent conductive front contact

This principal layer of the solar cell structure is both important and challenging due to the trade-off between electrical and optical requirements. From electrical point of view it has to be sufficiently conductive in order to reduce efficiency losses and provide ohmic contact to the buffer layer, in order to collect the charge of the whole device. From optical point of view it must be highly transparent to allow maximum illumination of the active layers.

Finding materials which are able to comply with both requirements is not an easy task. For instance, metals are highly conductive but are not transparent while most transparent and easily processed materials such as plastics and glass are isolating. Only certain metal oxides, known as Transparent Conducting Oxides (TCO-s) and some polymers such as polyanilines, polypyrroles, polythiophenes, polyphenylenes, poly(p-phenylenevinylenes) and especially PEDOT, Poly(3,4-ethylenedioxythiophene [19]. In addition to the limited choice of materials, their properties are subject to very precise control of oxygen content and doping levels in order to obtain the desired high transparency and conductivity.

TCO-s is preferred for solar cell application because of their long-term stability under illumination, including low-wavelength radiation that can damage most polymers. The group includes some oxides of groups III (Sn, Al, Ga, In) and VIII (Cd, Zn, Cu). These materials are in fact semiconductors with very high energy gap (usually above 3eV) which guarantee high optical transmission in the region of cell operation. Generally, the resistivity values of these compounds is very high so they have to be doped in order to move the Fermi level towards the conduction band an increase the concentration of electrons [20].

For solar cell applications, the properties of the TCO usually have to meet the following requirements:

- Low sheet resistance in order to minimize the final series resistance of the device.
- High transmittance (more than 90% in the 400-900nm spectral range which would allow high photon flux towards the window material and the absorber.
- Good adherence to the preceding layers.

Chalcopyrite cells in most cases use aluminum-doped ZnO although in some indium-doped tin oxide (ITO) or Sn_2O:F are used. These materials are n-type due to oxygen vacancies and this guarantees electrical matching with the n-type buffer layer.

Typical deposition technique is sputtering from ceramic targets. Precise control of oxygen content is necessary in order to achieve optimal conductivity and transparency. Other deposition techniques which still are being investigated are laser ablation, spraying, and solution growth and sol-gel. A big limitation to low-cost techniques such as sol-gel is that they usually require high temperature in order to obtain good conductivity [21]. At the same time, the low thermal stability of the p-n junction in chalcopyrite devices makes it impossible to deposit the TCO-s at temperatures much above 200ºC.

II. Methodology

II.1 Sol-gel & Pechini process

The common name "sol-gel process" brings together a large group of methods for obtaining (synthesis) materials from solutions, in which the gel formation is present at one of the process stages. The most famous version of the sol-gel process is based on the processes of controlled hydrolysis of compounds, usually alkoxides $M(OR)_x$ (M = Si, Ti, Zr, V, Zn, Al, Sn, Ge, Mo, W, etc.) or corresponding chlorides, in an aqueous or organic medium, usually alcohol.

At the first stage of the sol-gel process the hydrolysis and polycondensation reactions lead to the formation of a colloidal solution, i. e. sol, of hydroxide particles whose size does not exceed several dozen nm. Increasing bulk concentration of the dispersed phase or other changes in external conditions (pH, solvent substitution) leads to the intense formation of contacts between particles and the formation of a monolithic gel, in which the solvent molecules are enclosed in a flexible, but fairly stable, three-dimensional grid formed by particles of hydroxides. Concentration of sols followed by gelation is carried out using dialysis, ultrafiltration, electrodialysis, evaporation at relatively low temperatures, or extraction. [22]

The sol-gel process may be described as: "Formation of an oxide network through polycondensation reactions of a molecular precursor in a liquid."

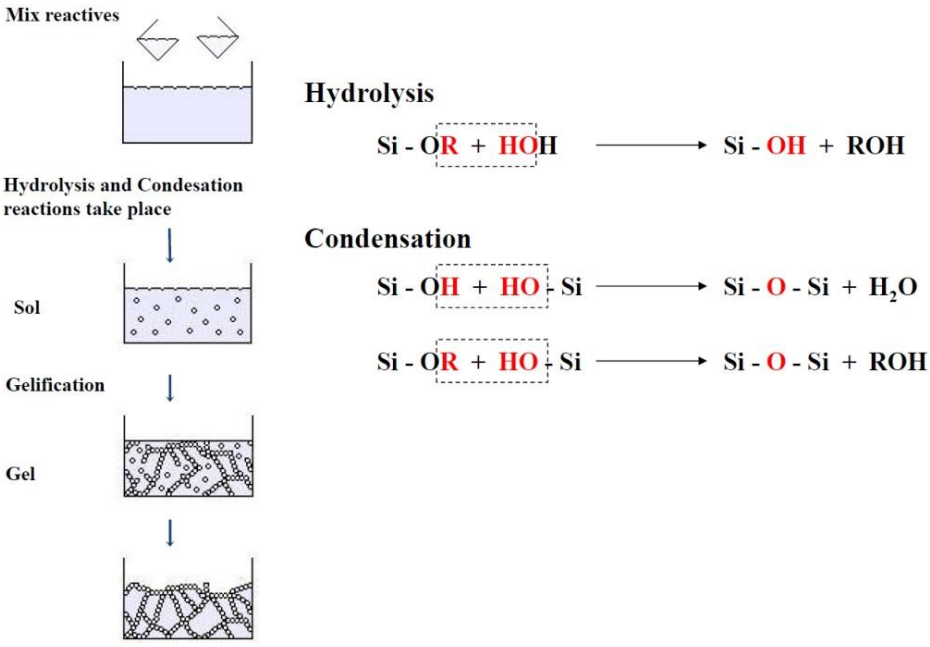

Figure 5. Mechanism of sol-gel process (silica gel)

The sol-gel process may be described as:"Formation of an oxide network through polycondensation reactions of a molecular precursor in a liquid."

A **sol** is a **stable dispersion of colloidal particles or polymers in a solvent**. The particles may be amorphous or crystalline. An aerosol is particles in a gas phase, while a sol is particles in a liquid.

A **gel** consists of a three **dimensional continuous network**, which encloses a liquid phase, in a colloidal gel, the network is built from agglomeration of colloidal particles. In a polymer gel the particles have a polymeric sub-structure made by aggregates of sub-colloidal particles. Generally, the sol particles may interact by van der Waals forces or hydrogen bonds. A gel may also be formed from linking polymer chains. In most gel systems used for materials synthesis, the interactions are of a covalent nature and the gel process is irreversible. The gelation process may be reversible if other interactions are involved.

•The idea behind sol-gel synthesis is to "dissolve" the compound in a liquid in order to bring it back as a solid in a controlled manner.

•Multi component compounds may be prepared with a controlled stoichiometry by mixing sols of different compounds.

•The sol-gel method prevents the problems with co-precipitation, which may be inhomogeneous, be a gelation reaction.

•Enables mixing at an atomic level.

•Results in small particles, which are easily sinterable.

Sol-gel synthesis may be used to prepare materials with a variety of shapes, such as porous structures, thin fibers, dense powders and thin films.

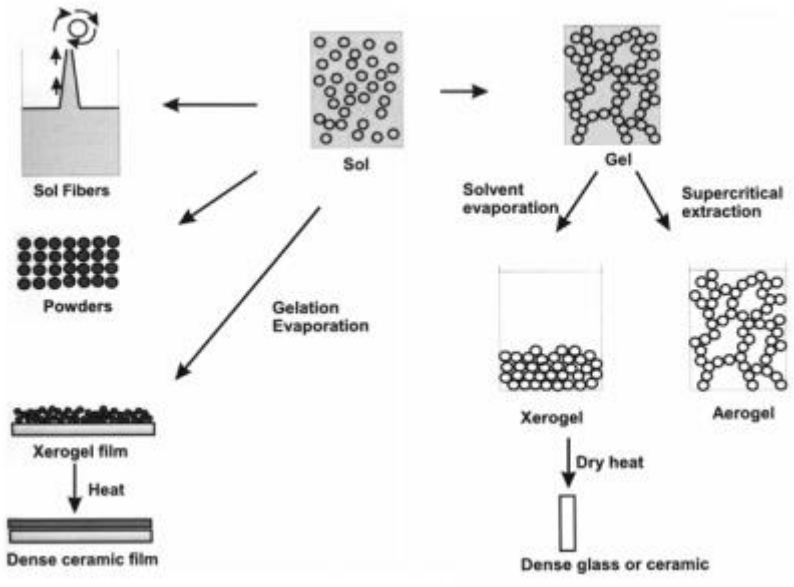

Figure 6. Sol-gel processing options

If the gel is dried by evaporation, then the capillary forces will result in shrinkage, the gel network will collapse, and a xerogel is formed.

If drying is performed under supercritical conditions, the network structure may be retained and a gel with large pores may be formed. This is called an aerogel, and the density will be very low. A record is < 0.005 g/cm^3. [23]

Pechini's method

The Pechini method was proposed in 1967 as a technique of depositing dielectric films of titanates and niobates of lead and alkaline-earth elements in the production of capacitors. Later, the process was customised for the in-lab synthesis of multicomponent finely dispersed oxide materials. The method is based on an intensive blending of positive ions in a solution, controlled transformation of the solution into a polymer gel, removal of the polymer matrix and development of an oxide precursor with a high degree of homogeneity.

During the synthetic process, *metal salts or alkoxides are introduced into a citric acid solution with ethylene glycol*. The formation of citric complexes is believed to balance the difference in individual behaviour of ions in solution, which results in a better distribution of ions and prevents the separation of components at later process stages. The polycondensation of ethylene glycol and citric acid starts above 100ºC, resulting in polymer citrate gel formation. When the heating temperature exceeds 400ºC, oxidation and pyrolysis of the polymer matrix begin, which lead to the formation of X-ray amorphous oxide and/or carbonate precursor. Further heating of this precursor results in the formation of the required material with a high degree of homogeneity and dispersion.

Today, the Pechini method is widely used in the synthesis of dielectric, fluorescent and magnetic materials, high-temperature superconductors and catalysts, as well as for the deposition of oxide films and coatings. The method's advantages include its relative simplicity, almost complete independence of the process conditions from the chemistry of positive ions contained in the final material and a relatively low temperature of precursor treatment, due to which the process may occur almost completely without sintering, resulting in the production of nanocrystal powders of refractory oxides. Shortfalls of the Pechini method include the use of toxic ethylene glycol and significant volumes of organic reagents per unit of product mass, a lack of stable citric complexes of some elements (bismuth, silicon, etc.), as well as the partial or complete regeneration of one of the components during pyrolysis of polymer gel (e.g., copper, lead, zinc, ruthenium, etc.). [24]

"Citric Acid"

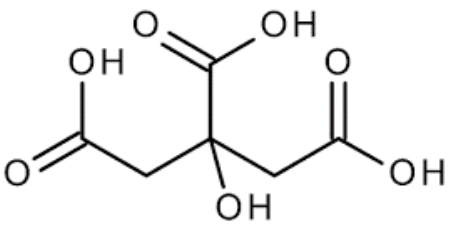

"Citrate"

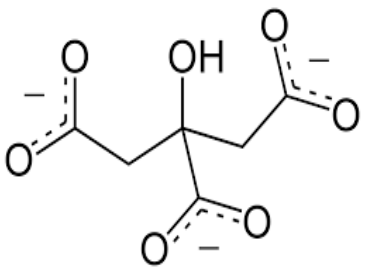

II.2 Solvothermal method

Solvothermal synthesis is a method for preparing a variety of materials such as metals, semiconductors, ceramics, and polymers. The process involves the use of a solvent under moderate to high pressure (typically between 1 atm and 10,000 atm) and temperature (typically between 100 °C and 1000 °C) that facilitates the interaction of precursors during synthesis.

If water is used as the solvent, the method is called "hydrothermal synthesis." The synthesis under hydrothermal conditions is usually performed below the supercritical temperature of water (374 °C). The process can be used to prepare a lot of geometries including thin films, bulk powders, single crystals, and nanocrystals. In addition, the morphology (sphere (3D), rod (2D), or wire (1D)) of the crystals formed is controlled by manipulating the solvent supersaturation, chemical of interest concentration, and kinetic control. The method can be used to prepare thermodynamically stable and metastable states including novel materials that cannot be easily formed from other synthetic routes. [25]

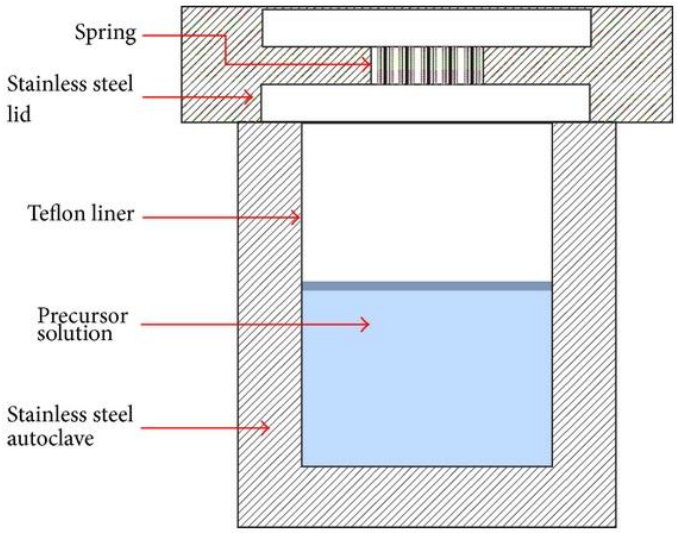

Figure 7. Hydro/Solvothermal reactor.

II.3 Co-precipitation synthesis

In the co-precipitation method, the salts are dissolved in water. A base solution is added into salt solution to precipitate the starting material. The precipitate is separated and sintered at desired temperature. The steps involved in co-precipitation are illustrated below (see Fig.8).

When concentration of a solute in the solvent exceeds its equilibrium solubility, a new phase i.e. supersaturation takes place. Without supersaturation no nucleation would occur. During chemical reactions, precipitation may also occur particularly if an insoluble substance is introduced into a solution and the density becomes greater (otherwise precipitate would float or form a suspension). With soluble substances, precipitation is accelerated once the solution becomes super saturated. [26]

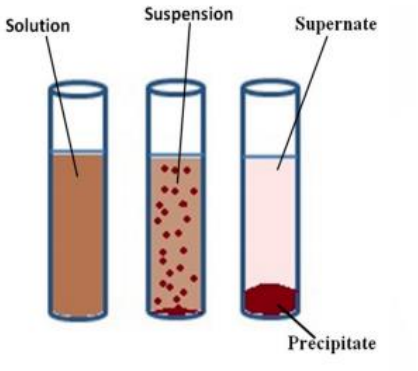

Figure 8. Co-precipitation

In the co-precipitation there are different factors to get precipitates of high reactivity:

a) Precipitant agent: the most frequent is use hydroxides by alkalize with ammonium. However, oxalates and sulfides are used when it is not possible the co-precipitation with hydroxides (the ions don't precipitate at the same pH). Depending on the started reagent (hydroxide, oxalate or sulfide), the results are so different.

b) Over-saturation, temperature and stirring conditions of the precipitate solution. Formation of colloids, specific surface and adsorbent properties of the precipitate can change in a significant way with these parameters. Normally, the best option is operating with a low over-saturation. A high temperature and stirring are needed to obtain small particle size and homogenous.

c) Contra-ions' type: chlorides and sulfates usually precipitate as a basic salt in many cases. Washing co-precipitates is a good way to stabilize the precipitate in his hydroxide, oxalate … although it is possible loses the stoichiometry by selective re-dissolution. [27]

Advantages

• Provides the only practical method of separation or concentration in some cases.

• Can be highly selective and virtually quantitative.

• High degree of concentration is possible.

• Provides a large range of scale (mg to industrial).

• Convenient, simple process.

• Carrier can be removed and procedure continued with tracer amounts of material (e.g., carrier iron separated by solvent extraction).

• Not energy- or resource-intensive compared to other techniques (e.g., solvent extraction).

Drawbacks

• Can be time consuming to digest, filter, or wash the precipitate.

• Precipitate can be contaminated by carrying of ions or postprecipitation.

• Large amounts of carrier might interfere with subsequent separation procedures.

• Co-precipitating agent might contain isotopic impurities of the analyte radionuclide.

• Scavenger precipitates are not as selective and are more sensitive to changes in separation procedures. [28]

III Coating techniques

Coating is the process of covering a substrate, with a product to alter and enhance its physical properties and appearance.

III.1 Dr. Blade (knife coating)

Doctor blade (or tape casting) is one of the widely used techniques for producing thin films on large area surfaces. Tape casting is a relatively new process which was originally developed during the 1940's as a method of forming thin sheets of piezoelectric materials and capacitors and is now an accepted precision coating method. One patent, issued in 1952, focuses on the use of aqueous and non aqueous slurries applied to moving plaster batts by a doctor blading device. In the doctor blading process, well-mixed slurry consisting of a suspension of ceramic particles along with other additives (such as binders, dispersants or plasticizers) is placed on a substrate beyond the doctor blade. When a constant relative movement is established between the blade and the substrate, the slurry spreads on the substrate to form a thin sheet which results in a gel-layer upon drying. The doctor blading can operate at speed up to several meters per minute and it is suitable to coat substrate with a very wide range of wet film thicknesses ranging from 20 to several hundred microns. There are two generally different coating devices in use: a doctor blade (e.g. a rectangular frame) and a spiral film applicator.

a) *Rectangular Frame*

This kind of doctor blade is also used in combination with a reservoir. The layer is formed by a doctor blade that is either stationary when used with a moving casting surface, or by a frame that moves along a stationary casting surface. Theprinciple is shown in figure 9.

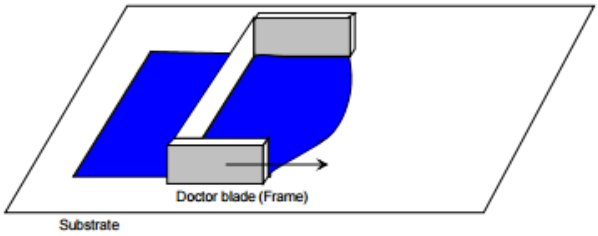

Figure 9. Principle of doctor blading using a frame with a reservoir of coating liquid which is moving relatively to the substrate.

The thickness of the layer is metered by adjusting the gap between the doctor blade and the substrate, as it is illustrated in figure 10.

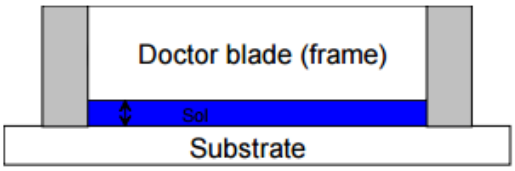

Figure 10. Wet layer thickness control by the gap between the frame and the blade

These blades provide very precise thickness control of the final layers. Doctor blade coating techniques are also used for coating plastic foils with coating liquids. In this case, the blade is positioned across a roll and the web is moved underneath the blade, as one can see from figure 11.

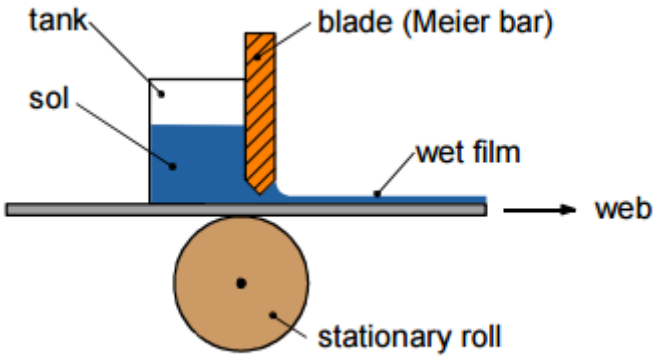

Figure 11. Doctor blade coating technique for plastic foil (Meier bar)

The gap between the blade and substrate can be adjusted by precision holders in the range of +/- 10 µm. The tank for the coating sol reservoir can be filled by continuous pumping, in order to avoid bubbles in the reservoir.

b) *Spiral film applicator*

The spiral film applicator is mostly used for coating foils, leather, textiles or other flexible materials with uneven surfaces. By using the spiral film applicator, the under-laying substrate is pressed down and flattened. The principle set-up is shown in figure 12.

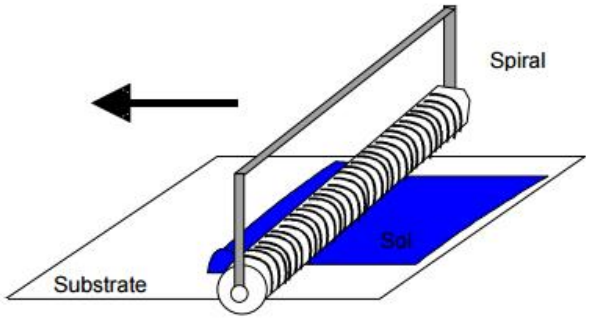

Figure 12. Principle set-up of doctor blading with a spiral film applicator.

The wet layer thickness is defined by the geometry and the size of the gaps, the spirals and the "gap-to-spiral-ratio" as one can see from figure 13.

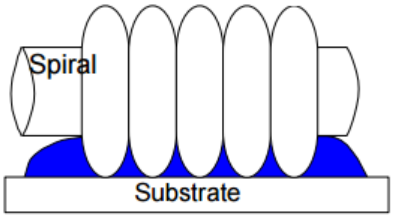

Figure 13. Demostration of the wet layer thickness control by the geometry and size of the gaps between the spiral and the "gap-to-spiral-ratio".

It is evident, that for both frame and spiral set-up, the wet film thickness is not only depending on the geometry of the coating device, but also on the wetting and the viscosity of the coating sol, as it is described below. [29]

Dr. Blade used during the synthesis was different because this material was not in the lab. The technique consisted in use sticky tape to immobilize the substrates. Furthermore, sticky tape is used for knowing the thickness of the layer.

III.2 Other deposition techniques

a) Spin coating

Spin coating is a procedure used to deposit uniform thin films to lat substrates. Usually a small amount of coating material is applied on the center of the substrate, which is either spinning at low speed or not spinning at all. The substrate is then rotated at high speed in order to spread the coating material by centrifugal force. A machine used for spin coating is called a **spin coater**, or simply **spinner**.

Rotation is continued while the fluid spins off the edges of the substrate, until the desired thickness of the film is achieved. The applied solvent is usually volatile, and simultaneously evaporates. So, the higher the angular speed of spinning, the thinner the film. The thickness of the film also depends on the viscosity and concentration of the solution and the solvent. A widely studied phenomenon in spin-coating is the coffee ring effect.

Spin coating is widely used in microfabrication of oxide layers using sol-gel precursors, where it can be used to create uniform thin films with nanoscale thicknesses. It is used intensively in photolithography, to deposit layers of photoresist about 1 micrometre thick. Photoresist is typically spun at 20 to 80 revolutions per second for 30 to 60 seconds.

b) Dip-coating

Dip coating is an industrial coating process which is used, for example, to manufacture coated fabrics and condoms. The earliest dip-coated products may have been candles. For flexible laminar substrates such as fabrics, dip coating may be performed as a continuous roll-to-roll process. For coating a 3D object, it may simply be inserted and removed from the bath of coating. For condom-making, a former is dipped into the coating. For some products, such as early methods of making candles, the process is repeated many times, allowing a series of thin films to bulk up to a relatively thick final object.

The final product may incorporate the substrate and the coating, or the coating may be peeled off to form an object which consists solely of the dried or solidified coating, as in the case of a condom.

As a popular alternative to Spin coating, dip-coating methods are frequently employed to produce thin films from sol-gel precursors for research purposes, where it is generally used for applying films onto flat or cylindrical substrates.

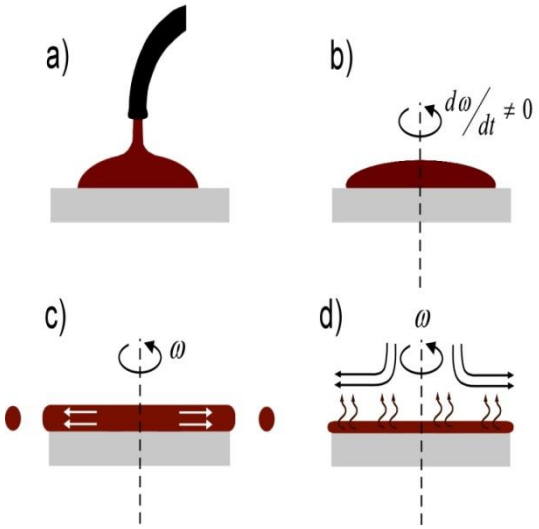

Figure 14. Spin coating process

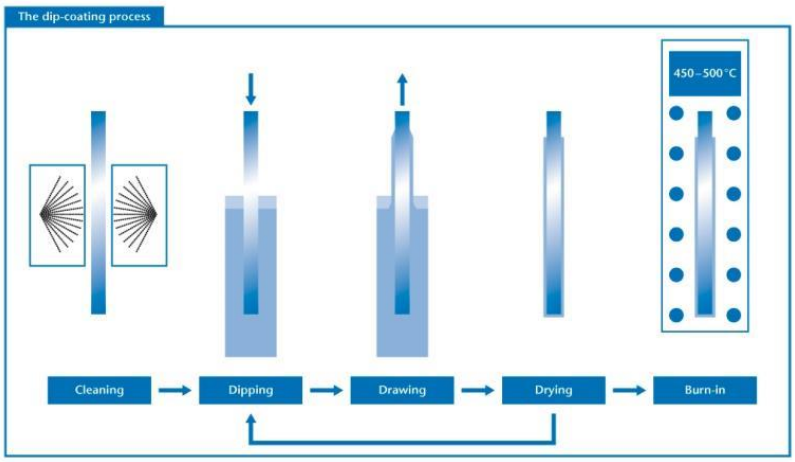

Figure 15. Dip-coating process

IV. Characterization techniques

IV.1 X-ray Diffraction (XRD)

X-ray diffraction (XRD) relies on the dual wave/particle nature of X-rays to obtain information about the structure of crystalline materials. A primary use of the technique is the identification and characterization of compounds based on their diffraction pattern.

The dominant effect that occurs when an incident beam of monochromatic X-rays interacts with a target material is scattering of those X-rays from atoms within the target material. In materials with regular structure (i.e. crystalline), the scattered X-rays

undergo constructive and destructive interference. This is the process of diffraction. The diffraction of X-rays by crystals is described by Bragg's Law, **nλ = 2d sinθ**. The directions of possible diffractions depend on the size and shape of the unit cell of the material. The intensities of the diffracted waves depend on the kind and arrangement of atoms in the crystal structure. However, most materials are not single crystals, but are composed of many tiny crystallites in all possible orientations called a polycrystalline aggregate or powder. When a powder with randomly oriented crystallites is placed in an X-ray beam, the beam will see all possible interatomic planes. If the experimental angle is systematically changed, all possible diffraction peaks from the powder will be detected.

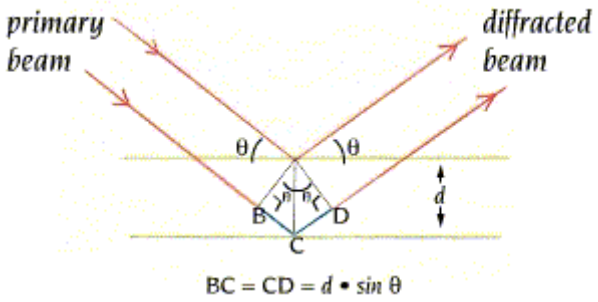

Figure 16 Bragg's Law

The parafocusing (or Bragg-Brentano) diffractometer is the most common geometry for diffraction instruments.

This geometry offers the advantages of high resolution and high beam intensity analysis at the cost of very precise alignment requirements and carefully prepared samples. Additionally, this geometry requires that the source-to-sample distance be constant and equal to the sample-to-detector distance. Alignment errors often lead to difficulties in phase identification and improper quantification. A mis-positioned sample can lead to unacceptable specimen displacement errors. Sample flatness, roughness, and positioning constraints preclude in-line sample measurement. Additionally, traditional XRD systems are often based on bulky equipment with high power requirements as well as employing high powered X-ray sources to increase X-ray flux on the sample, therefore increasing the detected diffraction signals from the sample. These sources also have large excitation areas, which are often disadvantageous for the diffraction analysis of small samples or small sample features.

Polycapillary X-ray optics can be used to overcome many of these drawbacks and constraints to enhance XRD applications. Polycapillary collimating optics convert a highly divergent beam into a quasi-parallel beam with low divergence. They can be used to form a Parallel Beam XRD instrument geometry which greatly reduces and removes many sources of errors in peak position and intensity inherent to the parafocusing geometry, such as sample position, shape, roughness, flatness, and transparency. Polycapillary focusing optics collects X-rays from a divergent X-ray source and direct them to a small focused beam at the sample surface with diameters as small as tens of micrometers for micro X-ray diffraction applications of small samples or small specimen features. Both types of polycapillary optics direct very high

X-ray intensities to the sample surface, such that XRD systems employing optics can use low power X-ray sources, reducing instrument size, cost, and power requirements.

X-ray diffraction using X-ray optics has been applied to many different types of applications including thin film analysis, sample texture evaluation, monitoring of crystalline phase and structure, and investigation of sample stress and strain. [30]

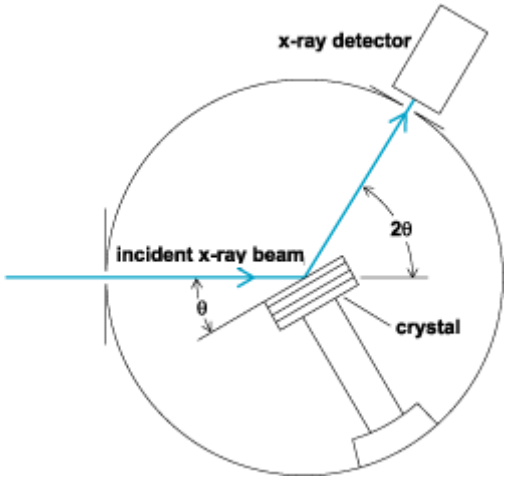

Figure 17. Scheme of how diffractometer works

IV.2 Scanning Electron Microscopy (SEM)

The scanning electron microscope (SEM) uses a focused beam of high-energy electrons to generate a variety of signals at the surface of solid specimens. The signals that derive from electron-sample interactions reveal information about the sample including external morphology (texture), chemical composition, and crystalline structure and orientation of materials making up the sample. In most applications, data are collected over a selected area of the surface of the sample, and a 2-dimensional image is generated that displays spatial variations in these properties.
Areas ranging from approximately 1 cm to 5 microns in width can be imaged in a scanning mode using conventional SEM techniques (magnification ranging from 20X to approximately 30,000X, spatial resolution of 50 to 100 nm). The SEM is also capable of performing analyses of selected point locations on the sample; this approach is especially useful in qualitatively or semi-quantitatively determining chemical compositions (using EDS), crystalline structure, and crystal orientations (using EBSD).

Accelerated electrons in an SEM carry significant amounts of kinetic energy, and this energy is dissipated as a variety of signals produced byelectron-sample interactions when the incident electrons are decelerated in the solid sample. These signals include secondary electrons (that produce SEM images), backscattered electrons (BSE), diffracted backscattered electrons (EBSD that are used to determine crystal structures and orientations of minerals), photons (characteristic X-rays that are used for elemental analysis and continuum X-rays), visible light (cathodoluminescence–CL), and heat. Secondary electrons and backscattered electrons are commonly used for imaging samples: secondary electrons are most valuable for showing morphology and topography on samples and backscattered electrons are most valuable for illustrating contrasts in composition in multiphase samples (i.e. for rapid phase discrimination). X-ray generation is produced by inelastic collisions of the incident electrons with electrons in discrete ortitals (shells) of atoms in the sample. As the excited electrons return to lower energy states, they yield X-rays

that are of a fixed wavelength (that is related to the difference in energy levels of electrons in different shells for a given element). Thus, characteristic X-rays are produced for each element in a mineral that is "excited" by the electron beam. SEM analysis is considered to be "non-destructive"; that is, x-rays generated by electron interactions do not lead to volume loss of the sample, so it is possible to analyze the same materials repeatedly.

Essential components of all SEMs include the following (see Fig.18):

- ElectronSource ("Gun")
- ElectronLenses
- SampleStage
- Detectors for all signals of interest
- Display / Data output devices
- InfrastructureRequirements:

    - PowerSupply
    - VacuumSystem
    - Coolingsystem
    - Vibration-free floor
    - Room free of ambient magnetic and electric fields

SEMs always have at least one detector (usually a secondary electron detector), and most have additional detectors.

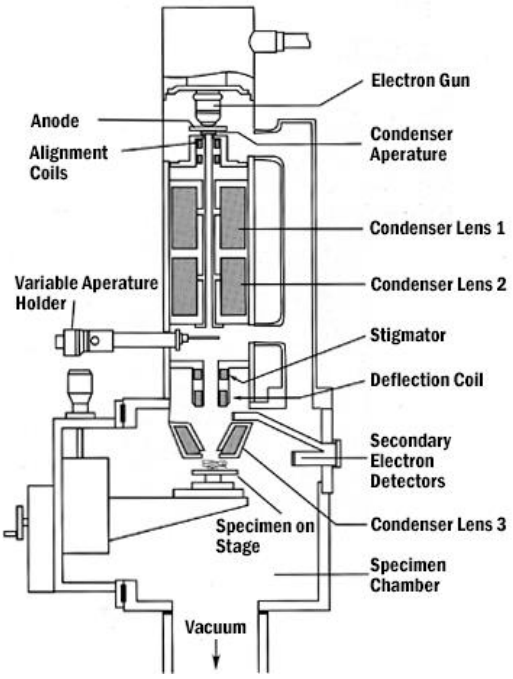

Figure 18. Different SEM parts

- Strengths

  There is arguably no other instrument with the breadth of applications in the study of solid materials that compares with the SEM. The SEM is critical in all fields that require characterization of solid materials. While this contribution is most concerned with geological applications, it is important to note that these applications are a very small subset of the scientific and industrial applications that exist for this instrumentation. Most SEM's are comparatively easy to operate, with user-friendly "intuitive" interfaces. Many applications require minimal sample preparation. For many applications, data acquisition is rapid (less than 5 minutes/image for SEI, BSE, spot EDS analyses.) Modern SEMs generate data in digital formats, which are highly portable.

- Limitations

  Samples must be solid and they must fit into the microscope chamber. Maximum size in horizontal dimensions is usually on the order of 10 cm, vertical dimensions are generally much more limited and rarely exceed 40 mm. For most instruments samples must be stable in a vacuum on the order of 10^{-5} - 10^{-6} torr. Samples likely to outgas at low pressures (rocks saturated with hydrocarbons, "wet" samples such as coal, organic materials or swelling clays, and samples likely to decrepitate at low pressure) are unsuitable for examination in conventional SEM's. However, "low vacuum" and "environmental" SEMs also exist, and many of these types of samples can be successfully examined in these specialized instruments. EDS detectors on SEM's cannot detect very light elements (H, He, and Li), and many instruments cannot detect elements with atomic numbers less than 11 (Na). Most SEMs use a solid state x-ray detector (EDS), and while these detectors are very fast and easy to utilize, they have relatively poor energy resolution and sensitivity to elements present in low abundances when compared to wavelength dispersive x-ray detectors (WDS) on most electron probe microanalyzers (EPMA). An electrically conductive coating must be applied to electrically insulating samples for study in conventional SEM's, unless the instrument is capable of operation in a low vacuum mode. [31]

IV.3 UV-Vis / NIR Spectroscopy

In this section it will explain how determine the band gap knowing the absorbance of the solid.
A way to study semiconductor's behaviour consists in the emission of photons which excites the electrons from low energy states to higher energy states overtaking the band gap energy (E_g). For this it can be used a system measurement of optic transmission to know the transmission coefficient of a slim semiconductor sample. The instrument is known with the name of spectrophotometer.

The principle of measurement consists in trough monochromatic radiation over the semiconductor sample. The spectrophotometer has a monochromator to filter light which wavelength is well defined. When the photons' energy favours the excitation of the electrons a changed in the signal of transmission is observed.

The semiconductor samples have to be slim to increase the sensitive of the measurements. The thickness have to be less than 0,5 mm.

If incident monochromatic light wavelength **λ** and intensity $\mathbf{I_0}$ on a sample which thickness is x emerges a transmitted intensity **I**. transmission coefficient is defined $\mathbf{T = I / I_0}$, related to the optical absorption coefficient α by:

$$T = \frac{(1-R)^2 \exp(-\alpha x)}{1-R^2 \exp(-2\alpha x)} \quad \text{(Eq. 1)}$$

"R" is the optic reflexion coefficient of the interface air-semiconductor.

The predominant mechanism of absorption is the transitions between the valance and conductive bands. If the semiconductor has direct gap, that is, if an incident photon only creates an electron-hole pair, the absorption coefficient is given by:

$$\alpha = A(E - E_g)^{1/2} \quad \text{(Eq. 2)}$$

"A" is a constant which depends on the material and "E" is the incident photon energy and the relationship is right in the approximation of parabolic bands, is that, the energy can be expressed as $E(p) \approx p^2$, "p" is the moment. However, if there is not a approximation with a parabolic bands (perhaps because of impurities or effect with the temperature) the coefficient is given by:

$$\alpha = B \exp(E / E_0) \quad \text{(Eq. 3)}$$

"B" is a constant and E_0 measures the separation of the parabolic form.

On the other hand, if the semiconductor has an indirect gap, to realize the electronic transmission a phonon with energy E_p has to involve conserving the moment (absorbing or emitting it). In this case the coefficient is given by:

$$\alpha = \alpha_a + \alpha_e \quad \text{(Eq. 4)}$$

"α_a" describes the absorption with the absorption of one phonon and "α_e" the absorption with emission of one phonon:

$$\alpha_a = C(E - E_g + E_p)^2, \quad E > E_g - E_p \quad \text{(Eq. 5a)}$$

$$\alpha_e = D(E - E_g - E_p)^2, \quad E > E_g + E_p \quad \text{(Eq. 5b)}$$

"C" and "D" are constants which depend on the material and temperature.

Therefore, if the transmission coefficient T is measured in terms of incident photon energy and Eq.1, the α coefficient is obtained from the dependence of this coefficient with the energy can deduce the nature of the energy band prohibited, that is, if the gap is directly or indirectly obtained Eg value and study, as appropriate, the phonon energy involved in the optical transition.

Chapter-2

V. Objectives

The main objectives of this project are:

- Synthesis of p-type semiconductor CuInxGa(1-x)Se_2 (CIGS) compound for use as absorber material for thin film solar cells.
- Preparation of CIGS by different non-vacuum routes like sol gel, solvothermal and co-precipitation methods.
- Deposition of the precursor paste by Dr. Blade technique-easy, low-cost and large scale method of covering.
- Studding of different synthesis's parameters to determine the optimal preparation condition.
- Evaluation the viability of the preparation procedure.
- Characterization of the obtained material to determine it structure, microstructure and optical properties.

VI. Experimental procedure

In this sub-chapter the methodology of the material preparation for each type of synthesis is explained.

The stoichiometry of the selected compound is $CuIn_{0,7}Ga_{0,3}Se_2$. The selection is based on previous studies exposed in the literature [12]. The atomic ratio of the metal cations is shown here after:

$$\frac{Cu}{In+Ga} = 0{,}9 \quad ; \quad \frac{Ga}{Ga+In} = 0{,}3$$

VI.1 Sol-gel process

The following raw materials are used for the sol-gel process (Table 2).

a) Raw materials

Table 2. Raw materials used for sol-gel route

Formula	MW (g/mol)	ρ (g/ml)	Purity
$C_3H_8O_2$	76,09	0,965	99,8%
C_2H_7NO	61,08	1,012	≥99,0%
$Cu(CH_3COO)_2$	199,65	X	>98%
$In(CH_3COO)_3$	291,96	X	99,99%
$Ga(C_5H_8O_2)_3$	367,05	X	99,99%
Se (elemental)	78,96	X	>99,5%

b) Synthesis procedure

The methodology is explained by steps as follow:

1) Weight on the raw materials.
2) Mixing of 1,8 ml of 2-metoxyethanol ($C_3H_8O_2$) with 0,132 g of gallium acetilacetate and 0,312 g of indium acetate and 0,4 g of copper acetate.
3) Stirring until a homogenous sol was reached.
4) We need a surfactant to get a good adhesion to the substrate. The surfactant used was monoethanolammine (MEA; C_2H_7NO). The literature says that the optimum amount of MEA is between 4 and 5%. For this reason we have measured 4,5% v/v (85 µl) of MEA for our mixture.
5) The obtained paste was homogenized in ultrasound bath for 15 minutes (to obtain a good dispersion).
6) Dr. Blade method with a device shown in the Figure 18 was used to coat the substrate.

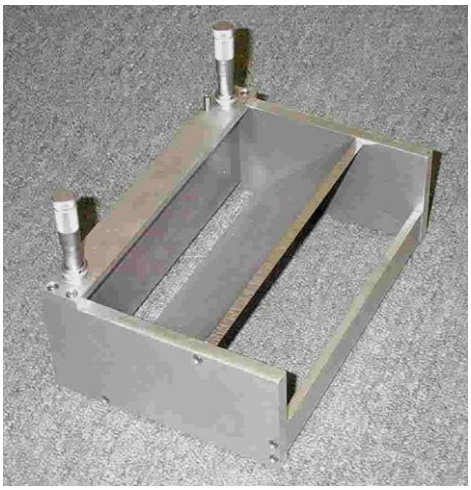

Figure 18. Dr. Blade instrument

7) Flat glass (Menzel-glaser) was used as substrates. Prior to deposition, the substrates were ultrasonically cleaned in a water-detergent solution, and then washed with distilled deionized water and ethanol.
8) After that, the substrate is heated at 400 ºC during 1 minute to remove partially the organic solvents and to enhance the crystallization process.
9) Finally, the sample is heated in a tubular furnace with Ar /Se atmosphere. The thermal treatment is explained hereafter.

c) Thermal treatment (Selenization)

The thermal treatment is made in a tubular furnace (Figure 19) according the cycle:

1) Heating rate of 20 ºC/min until reaches 525 ºC.
2) The furnace maintains the target temperature (525 ºC) during 45 minutes.
3) Finally, the furnace is free cooled up to room temperature.

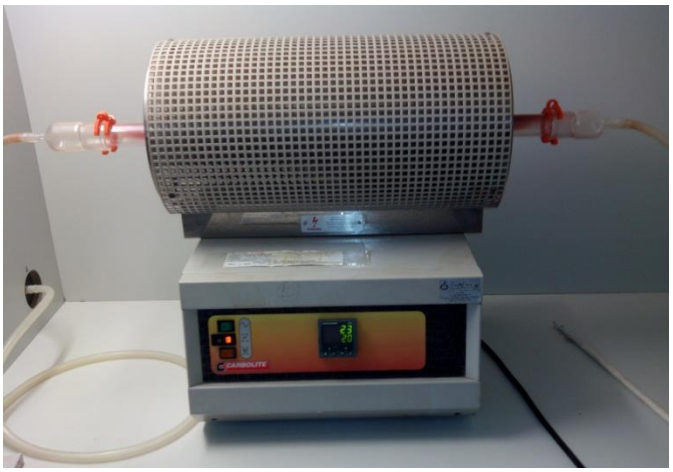

Figure 19. Tubular furnace used in the synthesis procedure.

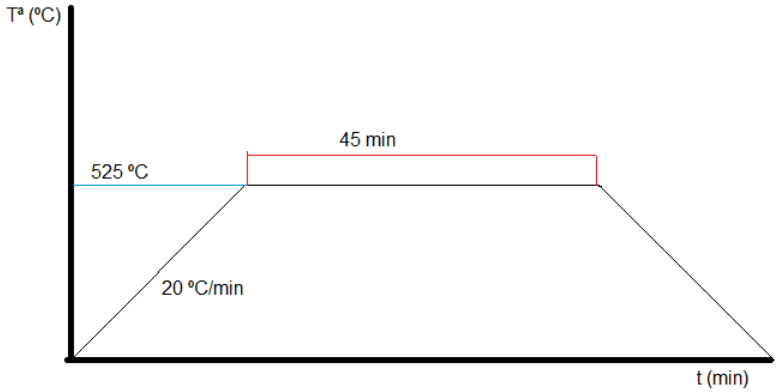

Figure 20. Schematical layout of the thermal cycle.

Before heating, the furnace is previously purged with (H_2/ N_2 5%) to ensure reductive atmosphere. Elemental selenium is placed inside the furnace in separate crucible with the intention to create saturate Se vapour that will avoid vacancies in the structure. Selenium tends to volatized at those temperatures. The thermal treatment procedure is the same for all methods of preparation and further explanation will be omitted here after.

During the thermal treatment the oxides are converted in metal selenides. The resulting thin film is further characterized.

VI.2 Pechini process

a) Raw materials

Table 3. Raw materials for Pechini process

Formula	MW (g/mol)	ρ (g/ml)	Purity
$Cu(NO_3)_2$ $3H_2O$	241,6	X	99%
$Ga(NO_3)$ $8H_2O$	399,74	X	99,9%
$In(NO_3)$ xH_2O	300,83	X	99,99%
$C_6H_{15}NO_3$ (TEA)	149,19	1,124	>99%
$HOC(COOH)(CH_2COOH)_2$	192,13	X	≥99,5%
$C_2H_6O_2$	62,07	1,113	>99%
C_2H_5OH (EtOH)	46,07	0,79	>99,8%

b) Synthesis

The mechanism of Pechini´s process is given in Figure 21.

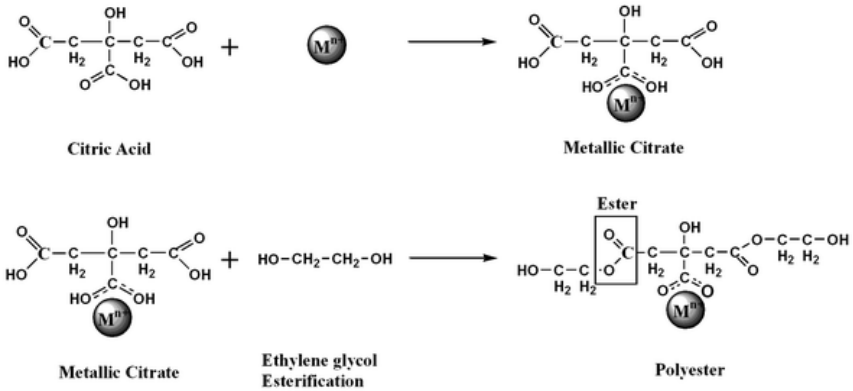

Figure 21. Pechini's mechanism.

The same stoichiometry is used for all methods. The amount of citric acid ($HOC(COOH)(CH_2COOH)_2$) and ethilenglycol ($C_2H_6O_2$) is selected according the stoichiometry and the following ratio:

$$\frac{n_{EG}}{n_{cit.ac}} = 2$$

Methodology:

1) Dissolving separately the $Cu(NO_3)_2$ $3H_2O$, $In(NO_3)$ xH_2O and $Ga(NO_3)$ $8H_2O$ in 10ml of distilled water for each one. This step is selected to avoid any possible precipitation.

2) Then, the three dissolutions are mix together. Citric acid is further added.

3) Stirring until the acid has been dissolve and then heat at 60 ºC.

4) Add 356 µl of EG (Ethilenglycol) and heat until 75 ºC during 2 hours.

5) Cooling at room temperature for 24 hours.

6) Heating to remove the remained water.

7) Pre-heating at 280 ºC during 6 hours using a heater.

8) The resulting powder is mixed with 0,35 ml EtOH and 80 µl of TEA.

9) Deposition by Dr. Blade.

10) Thermal treatment according the standard procedure.

11) Characterization of the obtained materials.

VI.3 Solvothermal

a) Raw materials

Table 4. Raw materials used in the solvothermal process.

Formula	MW (g/mol)	ρ (g/ml)	Purity
$Cu(NO_3)_2$ $3H_2O$	241,6	X	99%
$Ga(NO_3)$ $8H_2O$	399,74	X	99,9%
$In(NO_3)$ xH_2O	300,83	X	99,99%
SeO_2	110,96	X	99,8%
$C_2H_8N_2$ (en)	60,10	1,113	>99%
$C_6H_{14}S$ (hxSH)	118,2	0,84	96%

b) Synthesis

1) In 20 ml of distilled water is dissolved 0,2897 g of $Ga(NO_3)$ $8H_2O$, 0,5056 g of $In(NO_3)$ xH_2O and 0,5224 g of $Cu(NO_3)_2$ $3H_2O$.

2) Separately, 0,5247 g of SeO_2 and add 0,6 ml of ethylene di-amine were also dissolved.

3) Both dissolution were mixed together and introduced into the solvothermal reactor (Fig. 22) for 96 hours.
4) The resulting precipitate was mixed with 1 ml of hexathiol and stirring in an ultrasound bath during 15 minutes.
5) The sample is coated over the substrate and further the thermal treated.

Figure 22. Solvothermal reactor used in the process.

VI.4 Co-precipitation method

a) Raw materials

Table 5. Raw materials used in the co-precipitation method.

Formula	MW (g/mol)	ρ (g/ml)	Purity
$CuCl_2$ $2H_2O$	170,48	X	96%
$InCl_3$ $4H_2O$	293,24	X	97%
$Ga(NO_3)$ $8H_2O$	399,74	X	99,9%
NH_3	17,03	0,904	25%
$SeCl_4$	220,77	2,6	X
$C_6H_{14}S$ (hxSH)	118,2	0,84	96%

b) Synthesis

1) Mixing the precursor´s in distillate water.
2) Adding to the precursor dissolution 10 ml of ammonium 25%.
3) When the solution is get blue colour (due to the presence of Cu^{2+}), HCl (37%) is added carefully until the pH 5-6.
4) The precipitate is settled during 24 hours.
5) After, the solution is centrifuged (Fig. 23) and washed with distilled water and EtOH.
6) The removed water is used to detect the chloride ions. The test is made by adding a few drops of $AgNO_3$.
7) After complete washing, the powder is filtered and dried.
8) For deposition, paste made by 0,1 g of the obtained solid and 1 ml of hexathiol (hxSH) was mixing and dispersed in an ultrasound bath for 15 minutes.
9) The glass substrate is coated with the slip.
10) The sample is thermal treatment and finally characterized.

In order to evaluate the influence of precipitation agent, NaOH instead of NH_3 has been also tested using the same process. Image of the resulting powders is shown in Figure 24.

Figure 23. Centrifuge machine.

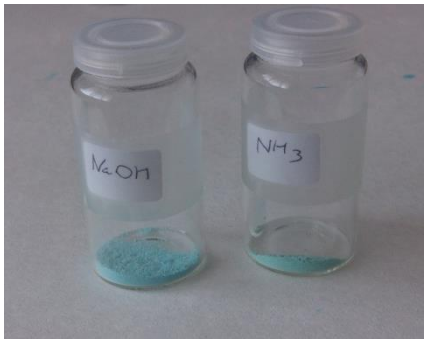

Figure 24. Precipitated powder (NaOH→ blue; NH_3→ green)

VII. Results and discussion

VII.1 Sol-gel

a) X-ray powder diffraction (DRX)

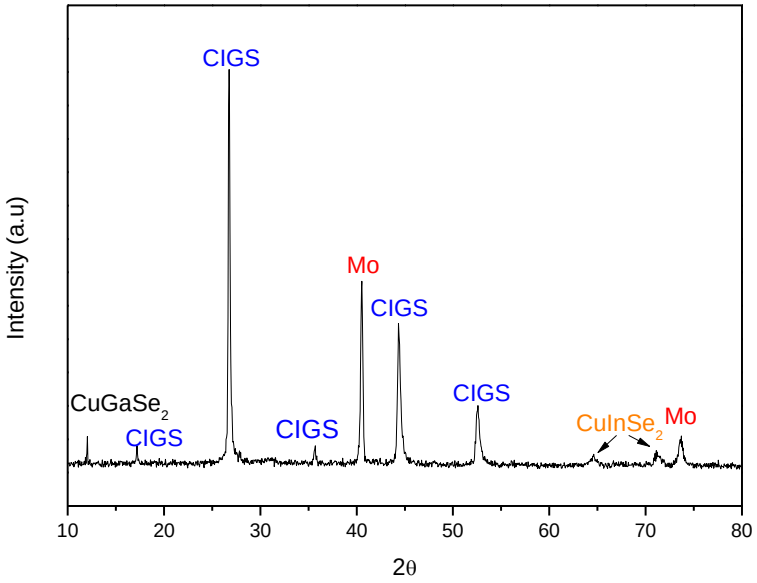

Figure 25. DRX of the sample made by sol-gel.

The obtained after thermal treatment thin film is characterized by DRX (Fig.25.).The diffractogram shows CIGS formation as a mayor crystalline phase. However, some secondary phases are also detected, as CuGaSe2 and CuInSe2. The reflection correspond to Mo is coming from the below back contact layer.

It have to be notified that the glass substrate covered with Mo conducting layer is used only for this sample, due to the lack of available quantity for the rest of the synthesized materials. However, this fact isn´t harm any properties or characterization results. The Mo covered substrate was selected with an intention to measure the electrical properties of the cell, e.g. conversion efficiency. Unfortunately, to complete the solar cell, specific equipment was needed that are not available in the Laboratory of the Solid State Chemistry Group at the University Jaume I.

b) Scanning Electron Microscopy (SEM)

The morphology of the resulting layer (Fig. 26) shows dense layer with some cracks in the surface. The particles have heterogeneous dimensions and distributions. The average size of the grain is between 5 and 12 µm. The image demonstrates some morphologically different crystals. The cross-section micrograph shows the support, Mo and absorber layer. The CIGS layer is about 2 µm.
The EDX analysis is made to check the elemental composition of the grains. Two different areas have been selected for EDX whose results are shown in Tables 6 and 7.

It can be observed from the Table 6 that the first area corresponds to Cu-poor composition, while the second analysed area (Table 7) has closed to the initial stoichiometry composition.

In conclusion, the CIGS is present as a major phase. The secondary phases seem to be as isolated particles as we didn't find differences in the composition corresponding

to that phases. Perhaps, changes in synthesis procedure are needed in order to obtain pure crystalline phase.

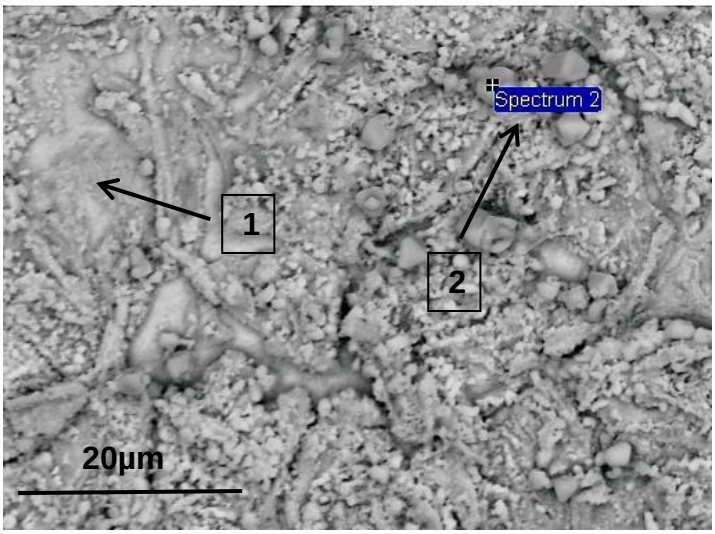

Figure 26 Sol-gel SEM (area)

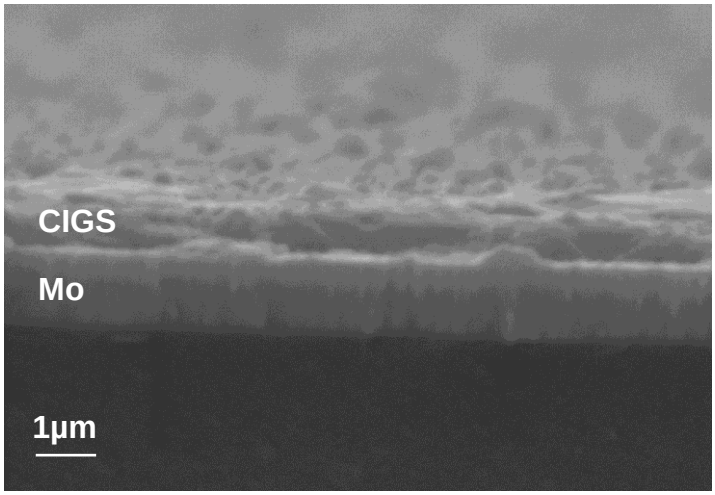

Figure 27. Transversal section of the sample.

Table 6. EDX analysis in area 1

Element	Atomic %	$\frac{Cu}{In+Ga}$	$\frac{Ga}{Ga+In}$
Cu	21,48	0,71	0,28
In	21,86		
Ga	8,49		
Se	48,16		

Table 7. EDX analysis in area 1

Element	Atomic %	$\frac{Cu}{In+Ga}$	$\frac{Ga}{Ga+In}$
Cu	29,17	1,05	0,32
Ga	8,77		
Se	42,99		
In	19,07		

c) UV-Vis-NIR

In the section IV.3 has been shown how to calculate the band gap knowing his absorption spectrum. Substitution of Ga for In in $Cu(In,Ga)Se_2$ enlarges the band gap between 1.22 to 1.34 eV, as a function of annealing temperature, with the change occurring primarily in the conduction band [32]. The fluctuation of the band gap value is due to the incorporation of Ga in different quantities in the crystal lattice, e.g. the formation of different solid dissolutions. The bandgap of CIGS varying continuously with x from about 1.0 eV (for copper indium selenide CuInSe2) to about 1.7 eV (for copper gallium selenide CuGaSe2)

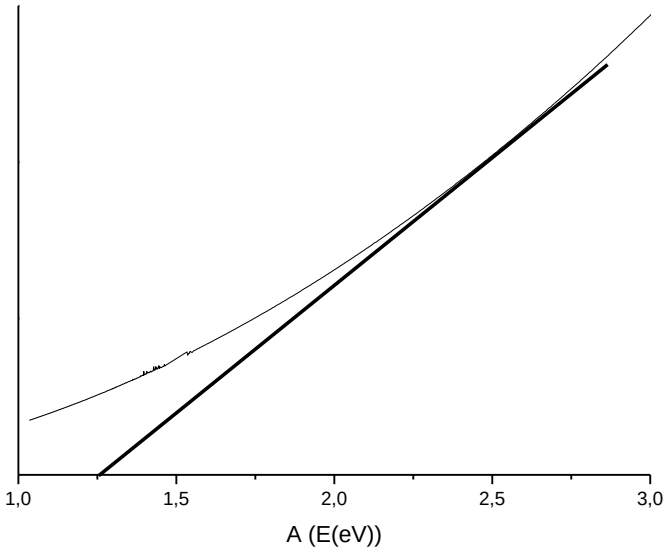

Figure 28 Band gap sol-gel process

As we can see the value for the band gap of our sample is 1,25 eV. This value fits with the solid dissolution designed for CIGS. The presence of secondary phases could modify slightly the optical properties of the layer. The obtained material is suitable for solar cell applications. However, to check if this statement is true, full assembly of the device is necessary.

VII.2 Pechini

a) DRX

The X-ray diffraction spectrum of the thin film layer shows three main reflections that fit with chalcopyrite phase. It can be observed that solid dissolution between $CuInSe_2$ and CIGS has been obtained. However, the sample is still amorphous as can be deduces from the background nature. The conclusion is that different thermal cycle is necessary to obtain well crystalized phase.

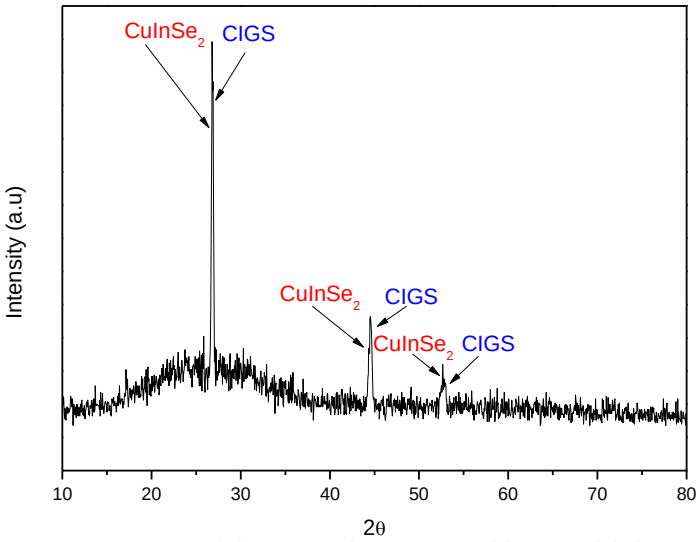

Figure 29 DRX spectrum of the sample prepared by Pechini method.

b) Scanning Electron Microscopy (SEM)

The SEM image in Fig. 31 shows particles with average dimensions 6µm distributed randomly. Some bigger grains of around 11µm can be also detected. The EDX analysis of the selected area (Table 8) shows Cu-reach phase composition.

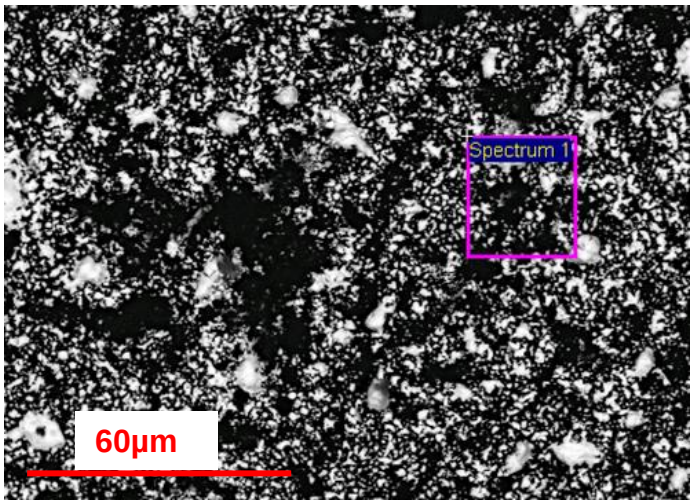

Figure 31. SEM image in backscattering mode.

Table 8. EDX of the area shown in the SEM image.

Element	Atomic %	$\frac{Cu}{In+Ga}$	$\frac{Ga}{Ga+In}$
Cu	31,03	1,21	0,25
In	19,26		
Ga	6,29		
Se	43,42		

c) UV-Vis-NIR

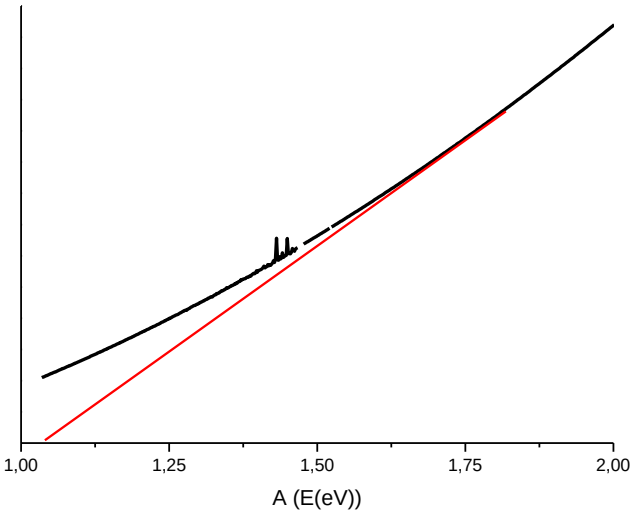

Figure 30 Band gap spectrum.

The obtained band gap for this sample is 1,05 eV. The value is lower than the corresponding to CIGS (1,22 eV). That means that the solid dissolution is not formed correctly. The composition is closed to $CuInSe_2$. This result fits with the DRX which showed that the phase of $CuInSe_2$ is present in the sample. This result suggests that Ga is in very small quantity or is not in the crystal lattice.

VII.3 Solvothermal

a) DRX

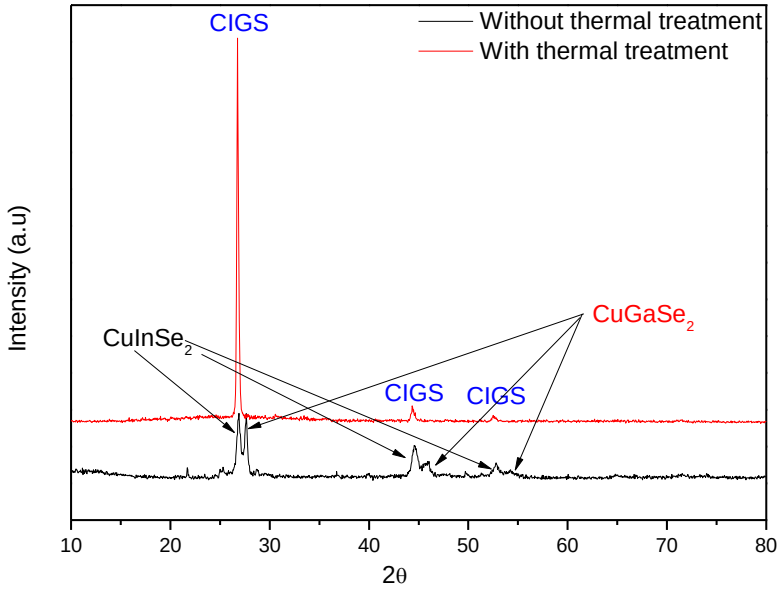

Figure 32. DRX of the sample prepared by solvothermal route. The red spectrum correspond to the calcined sample, while the black one to the as prepared.

The DRX spectra of the sample prepared by solvothermal route are shown in Figure 32. The as-prepared powder determined the existence of $CuInSe_2$ and $CuGaSe_2$ phases. The desired solid dissolution is not form at those experimental conditions. Only

after thermal treatment, the CIGS phase is appear as unique crystalline compound. However, the CIGS structure is deficient in gallium. The signals are between $CuInSe_2$ and $CuIn_{0,7}Ga_{0,3}Se_2$.

a) Scanning Electron Microscopy (SEM)

Dense and homogeneous layer is deduced from the SEM image in Fig. 34. The particles are small and regular distributed on surface. The biggest grains are around 9 µm, while the smallest ones are difficult to be measured as they are aggregated or very closed one to each other. However, most of the gains are ~ 2 µm. The chemical composition was checked by EDX (Table 9 and 10) and shows very similar to the initial stoichiometry composition.

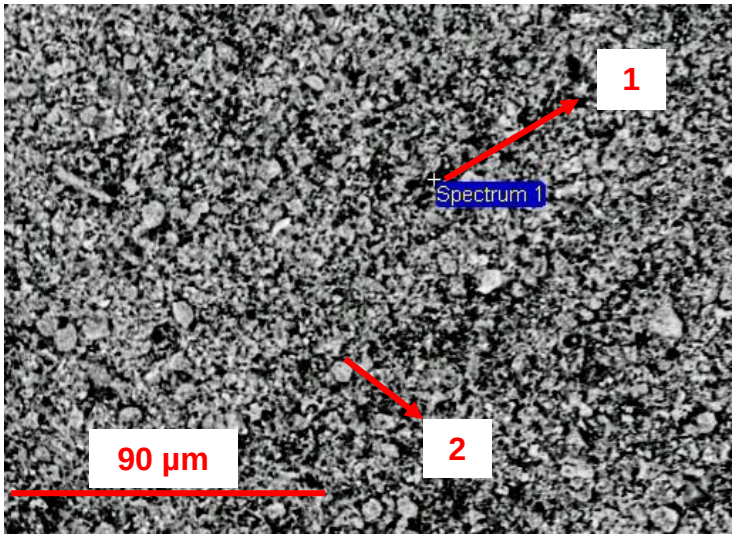

Figure 34. SEM image of the sample made by solvothermal route.

Table 9. EDX of area 1.

Element	Atomic %	$\frac{Cu}{In+Ga}$	$\frac{Ga}{Ga+In}$
Cu	25,80	1,00	0,29
In	18,24		
Ga	7,55		
Se	48,41		

Table 10. EDX of area 2.

Element	Atomic %	$\frac{Cu}{In+Ga}$	$\frac{Ga}{Ga+In}$
Cu	28,97	1,07	0,29
In	19,20		
Ga	7,93		
Se	43,90		

b) UV-Vis-NIR

In this case the value of the band gap is 1,12 eV. The result matches with the diffractogram (Fig.32). The band gap is higher than the band gap of CuInSe2 and it is

lower than the band gap of $CuIn_{0,7}Ga_{0,3}Se_2$. Thus, the solid dissolution is between both abovementioned compounds.

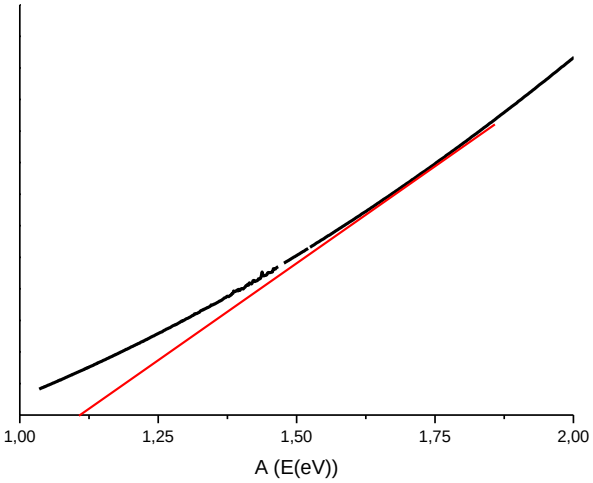

Figure 33. Band gap of the sample.

VII.4 Co-precipitation

a) DRX

The DRX results of both samples, with NH_3 and NaOH, CIGS has been obtained as major crystalline phase. Some impurities have been found as the presence of In_2O_3. Slightly better results can be detected for the sample prepared by the use of NH_3 as less intensity reflections of the secondary phase were observed. Thus, we can affirm that the use of ammonium as a precipitation agent is better than the NaOH.

For further characterization, only the sample with NH_3 will be used.

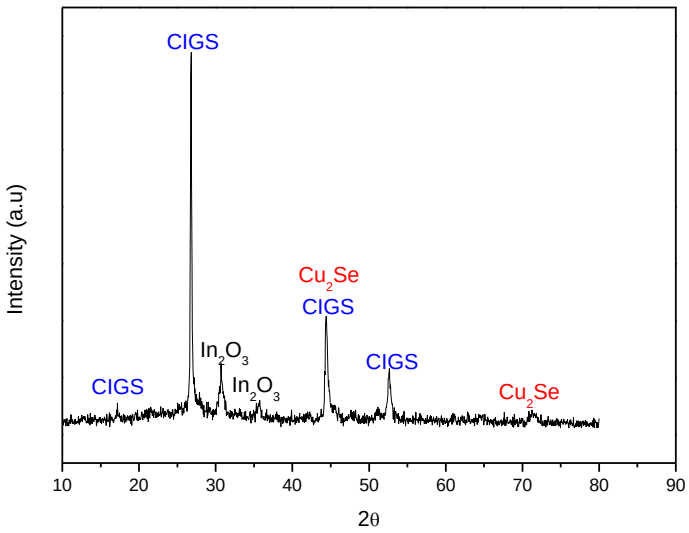

Figure 36 Co-precipitation DRX (NH_3)

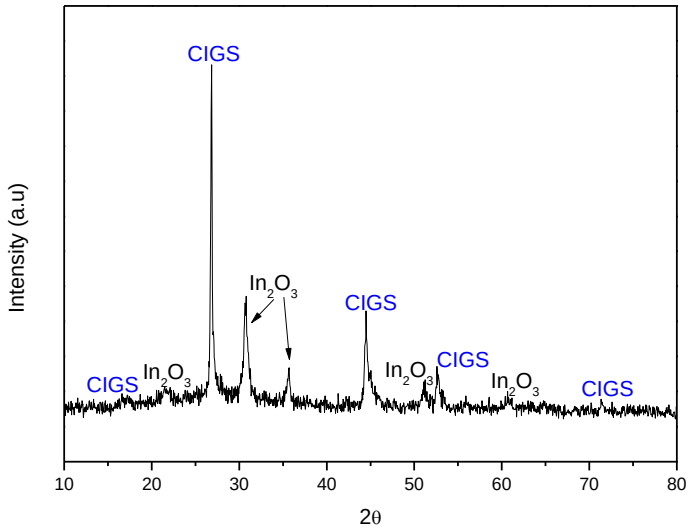

Figure 37 Co-precipitation DRX (NaOH)

b) SEM

The Figure 38 shows a compact layer with crystals of different size. The average size is 3 µm approximately, but it can be observed crystals of 6µm.

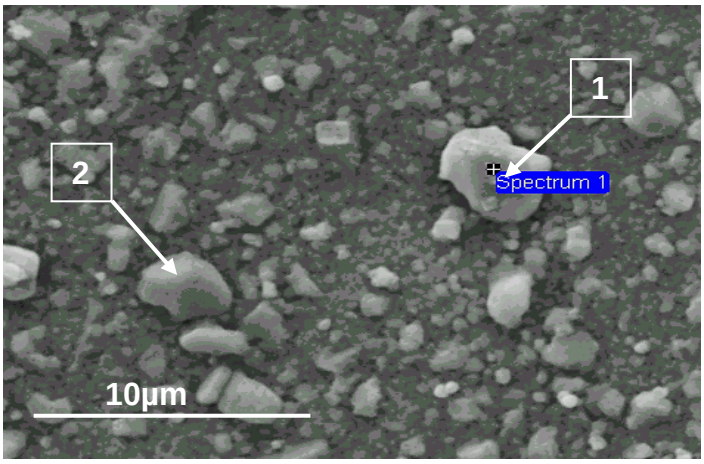

Figure 38. SEM image from the sample made by co-precipitation route. On the micrograph is labelled the areas analysed by EDX.

Table 11. EDX of area 1

Element	Atomic %	$\frac{Cu}{In+Ga}$	$\frac{Ga}{Ga+In}$
Cu	22,50	0,53	0,08
In	38,59		
Ga	3,58		
Se	35,32		

Table 12. EDX of area 2

Element	Atomic %	$\frac{Cu}{In+Ga}$	$\frac{Ga}{Ga+In}$
Cu	26,47	0,81	0,13
In	28,40		
Ga	4,23		
Se	40,90		

The chemical composition is checked by EDX (Table 11 and 12). The composition is different for both areas. The gain from Table 11 shows major presence of In, while the are analysed in Table 12 is closed to CIGS composition.

c) UV-Vis-NIR

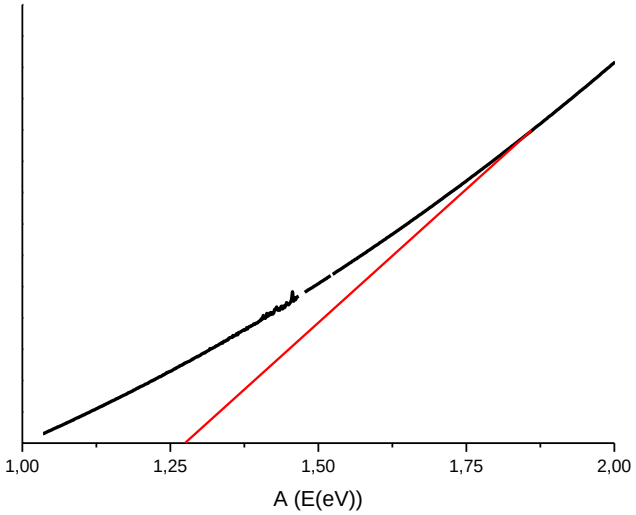

Figure 37. Band gap of the sample with NH_3.

The co-precipitation process give us a band gap of 1,28 eV. This is good results for CIGS and fit well with the solid dissolution designed.

Conclusions

- ✓ CIGS have been developed by most of the synthesis methods of preparations as a mayor crystalline phase.

- ✓ Better results regarding reactivity of the system correspond for the preparation routes of sol-gel and solvothermal.

  The use of NH_3 as a precipitation agent demonstrates better reactivity instead of NaOH.

- ✓ Morphologically, adequate microstructure for solar cell application is observed for the sample made by solvothermal route, due to the improved surface uniformity of the well distributes crystals with similar size.

- ✓ The optical properties of the studied sample show the existence of different solid dissolutions. The sample prepared by sol-gel exhibit band gap values closed to the desired compound.

  Thus, it can be concluded that the sample prepared by sol-gel route displays optimum characteristics as an absorber compound for solar cell applications compared with the rest of the studied samples.

V. Bibliography

[1] http://phys.iit.edu/~segre/phys100/science_2009_324_891.pdf

[2] Dye- sensitized solar cells, Edited by K. Kalyanasundaram, EPFL, Press, p. 8.

[3] A.Luque, S.Hegedus (Eds), Handbook of Photovoltaic Science and Engineering, John Wiley & Sons Ltd., 2003.

[4] M. A. Green, K. Emery, Y. Hishikawa and W. Warta, Solar Cells Efficiency Tables (Version 31), Prog. Photovoltaics: Res. Appl., vol.16, p. 61, 2008.

[5] Y. Tanaka, N. Akema, T. Morishita, D. Okumura, K. Kushiya, Improvement of Voc upward of 600 mV/cell with CIGS-based absorber prepared by Selenization/Sulfurization, Conf. Proceedings, 17th EC Photovoltaic Solar Energy Conference, Munich, p. 989, 2001.

[6] H. Hahn, G. Frank, W. Klingler, A. Meyer and G. Storger, Uber einige ternare Chalkogenide mit Chalkopyritstruktur. Z. Anorg. u. Allg.Chemie, vol. 271, p.153, 1953.

[7] S. Wagner, J. L. Shay, P. Migliorato and H. M. Kasper, CuInSe2/CdS Heterojunction Photovoltaic Detectors, Appl. Phys. Lett., vol.25, p.434, 1974.

[8] R. A. Mickelsen and W. S. Chen, High Photocurrent Polycrystalline Thin-film CdS/$CuInSe_2$ solar cell, Appl. Phys. Lett, vol.36, p.37, 1980.

[9] K. C. Mitchell, J. Ermer, and D. Pier, Single and tandem junction $CuInSe_2$ cell and module technology, Proc. 20th IEEE Photovoltaic Specialists Conf., Las Vegas, p. 1384,1988.

[10] T. Markvart, L. Castañar, (H.W. Schock) Practical Handbook of Photovoltaics, Oxford, ISBN 1856173909, 2003.

[11] F.J Haug, Development of Cu(in,Ga)Se2 Superstrate Thin Film Solar Cells. PhD Thesis. Zurich, 2001.

[12] T. Nakada, T. Kume, T. Mise A. Kunioka, Superstrate- Type Cu(In,Ga)Se_2 thin Film Solar Cell, Jpn. J. App. Phys. 37, p.499, 1998.

[13] J. Yun, K. Kim, M. Kim, B. Ahn, S .Ahn, J. Lee, K. Yoon, Fabrication of CIGS solar cells with a Na-doped Molayer on a Na-free substrate, Thin Solid Films, vol.515, p.5876, 2007.

[14] F. Kessler, D. Rudmann, Technological aspects of flexible CIGS solar cells and modules, Solar Energy, vol.77, p. 685, 2004.

[15] T. Nakada, Y. Hirabayashi, T. Tokado, D. Ohmori, T. Mise, Novel device structure for Cu(In,Ga)Se2 thin film solar cells using transparent conducting oxide back and front contacts, Solar Energy, vol.77, p. 739, 2004.

[16] D. Hariskos, S. Spiering, M. Powalla, Buffer layers in Cu(In,Ga)Se2 solar cells and modules, Thin Solid Films 480, p. 99, 2005.

[17] H.W. Schock, R. Noufi, CIGS-based Solar Cells for the Next Millennium, Prog. Photovolt. Res. Appl. 8, p. 151, 2000.

[18] R. Klenk, J. Klaer, D. Scheer, M. Lux-Steiner, I. Luck, N. Meyer, U. Ruhle, Solar cells based on $CuInS_2$—an overview, Thin Solid Films, p. 509, 2005.

[19] L. Groenendaal, F. Jonas, D. Freitag, H. Pielartzik, J. Reynolds, Poly(3,4-ethylenedioxythiophene) and Its Derivatives: Past, Present, and Future, Adv. Mater. 12(No.7), p. 481. 2000.

[20] C. Riuz Herrero, Modificación de las Propiedades Optoelectrónicas Por Medio del dopado con Bi en Células Fotovoltaicas Basadas en CdTe, Tesis Doctoral, Universidad Autonoma De Madrid, 2007.

[21] K. Lin, P. Tsai, Parametric study on preparation and characterization of ZnO:Al films by sol–gel method for solar cells, Materials Science and Engineering, vol.B, p.139, 2007.

[22] http://eng.thesaurus.rusnano.com/wiki/article847

[23]http://www.uio.no/studier/emner/matnat/kjemi/KJM5100/h06/undervisningsmaterial e/10KJM5100_2006_sol_gel_d.pdf

[24] http://eng.thesaurus.rusnano.com/wiki/article2075

[25] http://www.sigmaaldrich.com/technical-documents/articles/chemfiles/solvothermal-synthesis.html

[26] http://shodhganga.inflibnet.ac.in/bitstream/10603/9933/7/07_chapter%202.pdf

[27] G. Monrós, M. Llusar, J.A. Badenes. Química Inorgánica del estado sólido. Low-cost books, p.89, 2010.

[28] http://www.epa.gov/safewater/radionuclides/training/resources/MARLAP_14_8.pdf

[29] http://scidok.sulb.uni-saarland.de/volltexte/2011/3076/pdf/sm200405.pdf

[30] https://xos.com/technologies/xrd/

[31] http://serc.carleton.edu/research_education/geochemsheets/techniques/SEM.html

[32] S. Fiat, P. Koralli, E. Bacaksiz, K.P. Giannakopoulos, M. Kompitsas, D.E. Manolakos, G. Çankaya The influence of stoichiometry and annealing temperature on the properties of CuIn0.7Ga0.3Se2 and CuIn0.7Ga0.3Te2 thin films, 2013.

[33]O. Bondarchuck, Propiedades no-Óhmicas de materiales a base de óxido de indio como una de las líneas de investigación en el grupo GiiMCA, Revista Mexicana de Materiales Compuestos y Avanzados Posgrado, Universidad Tecnológica de la Mixteca, Huajuapan de León, Oaxaca México, C.P. 69000, vol.1 (No. 4), p.1, 2011.